Physics Letters A 378 (2014) 2635–2639

Contents lists available at ScienceDirect

Physics Letters A

www.elsevier.com/locate/pla

Tuning p/n conductivity in wurtzite transition metal monoxide: Role of native defects in CoO and MnO

Jian-Ming Wu [a], Li-Juan Chen [a], Xiao-Bao Yang [a], Yu-Jun Zhao [a,b,*]

[a] Department of Physics, South China University of Technology, Guangzhou 510640, People's Republic of China
[b] Key Laboratory of Advanced Energy Storage Materials of Guangdong Province, South China University of Technology, Guangzhou 510641, People's Republic of China

ARTICLE INFO

Article history:
Received 19 May 2014
Received in revised form 5 July 2014
Accepted 12 July 2014
Available online 15 July 2014
Communicated by R. Wu

Keywords:
CoO
MnO
Wurtzite structure
Intrinsic defects
p/n conductivity

ABSTRACT

First-principles calculations with GGA+U approach are carried out in studying the properties of intrinsic defects of the wurtzite MnO, and CoO. For intrinsic MnO, it shows tunable p-type and n-type conductivity under O rich and O poor conditions, respectively. For intrinsic CoO, it is easy to be designed as p-type semiconductors under O rich condition, but hard for n-type. We expect that the tunable p/n conductivity of MnO could open a new application prospect for the *wurtzite* semiconductor materials.

1. Introduction

Most of the transition metal (TM) monoxides have their ground states of rock salt (RS) structure, while few were found to be stable at wurtzite (WZ) structure [1,2]. In addition to the well-known ZnO, only two other TM monoxides, CoO in 1962 [3], and MnO in 2012 [4] were reported to be stabilized at WZ structures. Although ZnO have attracted much attention for several decades for its many remarkable properties including large band gap, high exciton binding energy, etc. [5–7], it is well known that a problem of p/n doping asymmetry often exists in such wide band gap (WBG) semiconductors [8–11]. Many researches reveal that the easy compensated dopants (or defects) and the deep defect level should mainly correspond to this issue [12–17]. Wei et al. are dedicated to reduce the ionization energies of dopants through proposing an impurity band model [12,14,18]. On the other hand, CoO and MnO, are applicable for electronic devices with ZnO, as they can be stabilized at WZ phase, though having relative lower band gaps around 1.6 eV [4,19]. The relative low energy gap helps avoiding the well-known doping asymmetry problem in WGS, and thus it holds a big promise to realize both n- and p-type conductivities in transition metal oxides of *WZ structure*.

As most of the ionic compounds have anion-derived valence band and cation-derived conduction band, anion vacancies and interstitial cations often act as donor defects, while cation vacancies and interstitial anions often act as accepter defects [15,16,20,21]. Despite the fact that the intrinsic lattice defect has critical influence on the p/n doping properties, no comprehensive discussion is available for CoO and MnO, the rare WZ transition metal monoxide besides the intensively studied ZnO.

In this work, we have evaluated the formation energies of various intrinsic defects for WZ CoO and MnO systems. We find that the WZ CoO is relatively easy to realize p-type conductivity, but hard for n-type conductivity. Interestingly, the WZ MnO can display both p- and n-type conductivities, as long as proper growth conditions are chosen (O-rich and Mn-rich for p- and n-types, respectively).

2. Computational details

First-principles calculations were performed using the projector-augmented wave method [22] as implemented in the Vienna *ab initio* simulation package (VASP) with based on density functional theory (DFT) [23–25]. The spin-polarized generalized gradient approximation (GGA) of the Perdew–Burke–Ehrenkof formulas (PBE) [26] and the effective Hubbard potentials with $U = 4$ [27] and 6 eV [4] for Co and Mn, respectively, are used through the calculations. For the 96-atom supercell, a regular k-mesh of $3 \times 3 \times 3$ and an energy cutoff of 400 eV are adopted to ensure an energy precise in

* Corresponding author at: Department of Physics, South China University of Technology, Guangzhou 510640, People's Republic of China. Tel.: +86 20 87110426; fax: +86 20 87112837.
E-mail address: zhaoyj@scut.edu.cn (Y.-J. Zhao).

http://dx.doi.org/10.1016/j.physleta.2014.07.015
0375-9601/

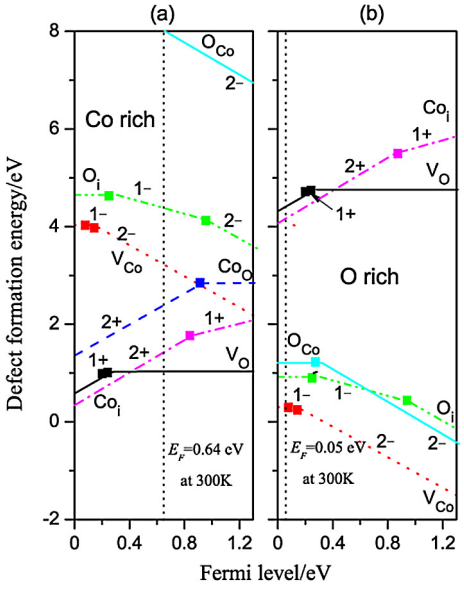

Fig. 1. (Color online.) Defect formation energies of CoO under Co rich (a) and O rich (b) conditions. The vertical dotted lines denote the corresponding calculated Fermi level at 300 K.

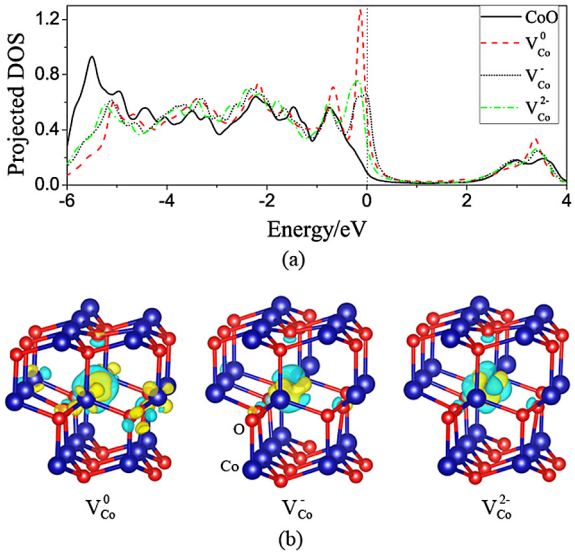

Fig. 2. (Color online.) (a) Projected density of states of O near V_{Co} as well as in the perfect CoO system. (b) Charge density difference of V^0_{Co}, V^-_{Co}, and V^{2-}_{Co}. The red and blue balls stand for the O and Co ions, respectively.

1 meV per formula for CoO and MnO. The defect formation energies are obtained with the definition proposed in previous works [28,29]. No extra correction is included since the errors related to the periodic boundary condition (PBC) are well converged in such a large supercell. Self-consistent calculation [30,31] are carried out for the Fermi level estimation.

3. Results and discussion

It is widely accepted that the GGA approach often fails to describe the exact structural and electronic properties related to the strongly correlated systems, such as TM monoxides [32,33]. In particular, theoretical description of the ground state of CoO and MnO is still an open question [34]. In this work, the relative total energies of CoO and MnO in zincblende structure (ZB) and wurtzite (WZ) structure with respect to corresponding rock-salt (RS) structures are calculated within GGA and GGA+U approaches for comparison. According to the GGA approaches, both CoO and MnO are energetically favored by −0.257 eV and −0.244 eV per formula in zincblende structure, while −0.178 eV and −0.201 eV in wurtzite structure, respectively, with respect to the well-established ground state of RS structure. Within GGA+U approach, the ground state of MnO turns to be NaCl-type structure with its relative energies of 0.089 eV and 0.093 eV for zincblende and wurtzite structure, respectively. However, GGA+U approach cannot describe CoO well as its relative energies decrease to −0.862 eV and −0.870 eV for zincblende and wurtzite structure, respectively. Within GGA+U approach, the calculated band gaps of 1.30 eV and 1.60 eV for CoO and MnO are in a reasonable range. Since neither GGA nor GGA+U could describe the ground state of MnO and CoO well, we do not consider their RS structure as competing phases in the determination of the chemical potential ranges, though some related discussions are given when necessary, such as the comment for the negative formation energy of V_O. Nevertheless, the calculated transition level of the defects is independent of the adopted chemical potentials.

3.1. CoO

The formation energies of various intrinsic defects of CoO system were shown in Fig. 1. Under O rich condition, the formation energies of the acceptor defects obviously get prevailed over that of the donor defects by at least 3 eV. The calculated effective masses at VBM and CBM are 2.44 and 5.81 m_e for hole (m^*_p) and electron (m^*_n), respectively. Consequently, the self-consistent calculated E_F is pinned at 0.05 eV above VBM at 300 K, as it is dominated by the defects of V_{Co}, O_i, and O_{Co}. All the compensated donor defects hardly exist since their formation energies are higher than 4 eV. The corresponding carrier calculated concentration is as high as 1.4×10^{19} cm^{-3}, showing good p-type conductivity. However, under Co rich condition, the calculated E_F is pinned at 0.64 eV from VBM, with an obvious deviation from the lowest cross point of the donor and the acceptor defects (Fig. 1(a)). This is understandable since the formation energy of the donor and acceptor at the lowest cross point is nearly above 2 eV, which leads to relatively low defect concentrations. As a result, the corresponding carrier concentration significantly influences the position of balanced Fermi level, though the net electron carrier concentration is only 3.02×10^7 cm^{-3}. Taking into account of the balanced Fermi level under both Co-rich and O-rich, we find that the WZ CoO system is relatively easy to be p-type doping, but hard for effective n-type doping, indicating that the issue of doping asymmetry exists in CoO system.

We have calculated the projected density of states (PDOS) as well as the charge density difference of V_{Co}, as shown in Fig. 2. Compared to the perfect CoO, V_{Co} induces the levels of dangling electrons of adjacent oxygen ions be more localized around the Fermi level. The defect levels are distributed near the VBM as shallow acceptor levels, in line with the results from the analysis of the defect formation energies as in Fig. 1. Significant band gaps are found in those four cases. From Fig. 2(b), we find that the oxygen ions around the V_{Co} are relaxed outward for all the three cases. The defect induced charge transfer occurring mainly in the vacancy site and also slightly in the first neighbor O sites, while it is also found in the first neighbor Co sites for V^0_{Co}. The relative localized charge transfer may be in corresponding to the appearance of the shallow acceptor levels.

3.2. MnO

The defect formation energies of MnO are shown in Fig. 3(a)–(c). Generally, the Mn rich condition is beneficial for the formation of donor defects, while the O rich condition favors the acceptor

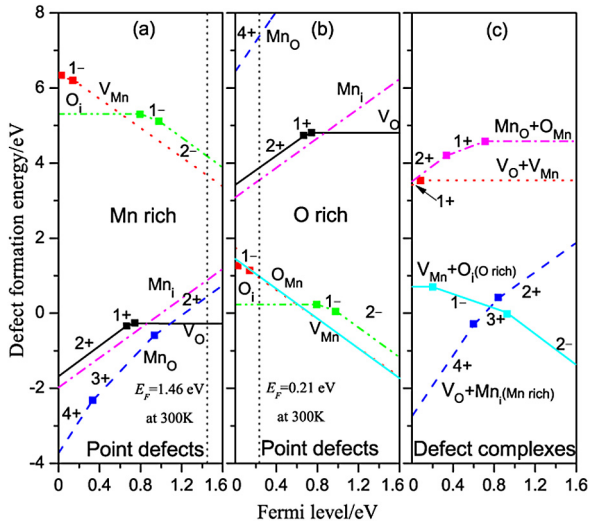

Fig. 3. (Color online.) Defect formation energies of point defects under Mn rich (a) and O rich (b) conditions, and defect complexes (c) of MnO under both Mn- and O-rich conditions. The formation energies of $V_O + Mn_i$ and $V_{Mn} + O_i$ are displayed with Mn rich and O rich, respectively, while that of other defect complexes are independent from the chemical potential conditions. The vertical dotted lines denote the corresponding calculated Fermi level at 300 K with both the point defects and the defect complexes are considered.

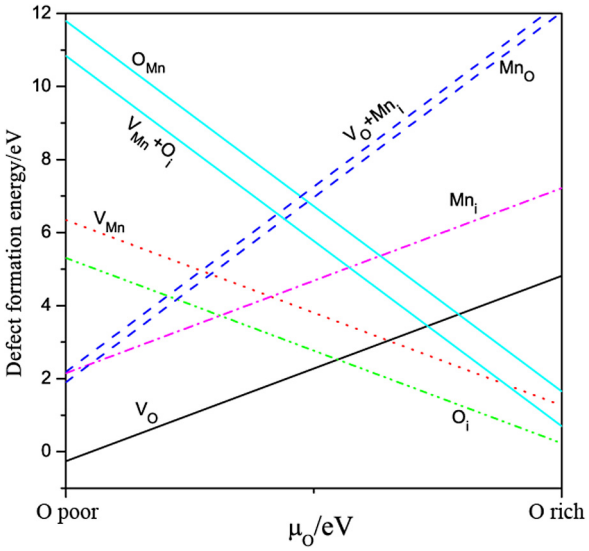

Fig. 4. (Color online.) The formation energies of various neutral charged defects with respect to the chemical potential of oxygen.

defects as no any remarkable compensative defects. As shown in Fig. 3(c), defect complexes of $V_O + Mn_i$ and $V_{Mn} + O_i$ are easily formed with low formation energies under Mn rich and O rich conditions, respectively. Other defect complexes are hardly formed due to their large formation energies. We notice that, the calculated formation energy of V_O is always negative as the Fermi level shifts from VBM to CBM under the Mn rich condition. It may result from the fact that the rock salt MnO is not considered as the competing phases here, and it implies that the extreme Mn rich condition may not be suitable for the preparation of WZ MnO.

Within a tetrahedral like crystalline field, the 3*d* electrons will split into an energetically lower triplet state of t_{2g} and a higher doublet state e_{2g}. According to the analysis in our early work [35], Mn and Co have an open t_{2g} and close e_{2g} structures in electronic configuration, respectively. The calculated cohesive energy of MnO (−5.615 eV) is much lower than that of CoO (−3.826 eV). This may be correlated to the fact that e_{2g} is much localized than t_{2g}, leading to a relative weak ionic interaction in CoO compared to that in MnO system. For MnO, the stronger interaction between Mn and O push the VBM into a deeper level than CoO system. As a result, at VBM, the formation energies of positive charged defects will decrease while that of negative charged defects will increase accordingly. This may mainly correspond to the difference of defect formation between CoO and MnO systems, i.e. the formation energy of V_{Co} is much lower than that of V_{Mn}. In addition, one needs to keep in mind that the formation energies are closely correlated to the chemical potentials of metals and the Fermi levels of the defect contained systems.

For a clearer description, the formation energies of different intrinsic defects with neutral charge state are chosen to display with respect to the chemical potential of oxygen (cf. Fig. 4). It is clear that the O poor condition is beneficial for the formation of the donor preferred defects, while the O rich condition is beneficial for the acceptor defects. In both extreme conditions, the corresponding compensative defects are well restrained due to their high formation energies. Near the O poor side, V_O is the dominate defect with a low formation energy. Other donor defects of Mn_i, Mn_O, and $V_O + Mn_i$ have relative high formation energies of about 2 eV, but are still much lower than that of the acceptor defects, such as O_i (5.301 eV at O poor point) and V_{Mn} (6.339 eV at O poor point). The concentrations of the defects of O_{Mn} and $V_{Mn} + O_i$ are negligible, since their formation energies are higher than 10 eV. Similar situations could be found in the O rich end. In the middle region, neither hole nor electron carrier would be significantly abundant since the donor and acceptor defects are rather balanced.

The Fermi levels determined by the self-consistent calculations, with consideration of both the point defects and the defect complexes, are denoted for Mn rich (Fig. 3(a)) and O rich (Fig. 3(b)) conditions, respectively. The m_p^* and m_n^* at VBM and CBM are calculated to be 2.43 and 0.61 m_e, respectively. Under Mn rich condition, E_F is pinned at 0.14 eV below CBM, a relatively shallow level for *n*-type conductivity. Around this region, the main defect is V_O, followed by Mn_O and Mn_i. In contrast, under O rich condition, E_F is pinned at 0.21 eV above VBM, a relatively shallow level for *p*-type conductivity, as O_i is the dominant defect, followed by O_{Mn} and V_{Mn}. For both of those two extreme conditions, the corresponding compensated defects are unlikely formed as their formation energies are greater than 3 eV. Obviously, the Fermi level could be regulated separately as shallow levels from both VBM and CBM through adjusting the chemical potentials of the growth condition, showing excellent controllable p/n doping properties.

The calculated carrier concentrations of MnO with consideration of the varied chemical potential conditions as well as the measuring temperature are shown in Fig. 5. Regions with *n*-type or *p*-type conductivity are clearly defined with respect to μ_O. At the O poor condition, the donor defects prevail in the defects, and thus leading to an *n*-type conductivity. As μ_O increasing from O poor to O rich condition, the Fermi level falls deep into the band gap, and the corresponding carrier concentration decreases consequently. When $\Delta\mu_O$ is located at the region in −3.53 to −1.53 eV, the carrier concentration falls down to below 10^7 cm^{-3}. As μ_O gets closing to the O rich side, the acceptor defects get prevailed to the donor defects and the Fermi level is located close to the VBM. A *p*-type conductivity is then highlighted. In certain degree, the measuring temperature would influence the carrier concentration by more than an order of magnitude. For instance, under O poor, the carrier concentrations change from 10^{11} to 10^{15} cm^{-3} as the temperature increasing from 50 K to 100 K, and even reach to 10^{19} cm^{-3} at 600 K. Obviously, through regulating the chemical potential environment, we could expected a feasible controlling of *p*-type or *n*-type conductivity for MnO.

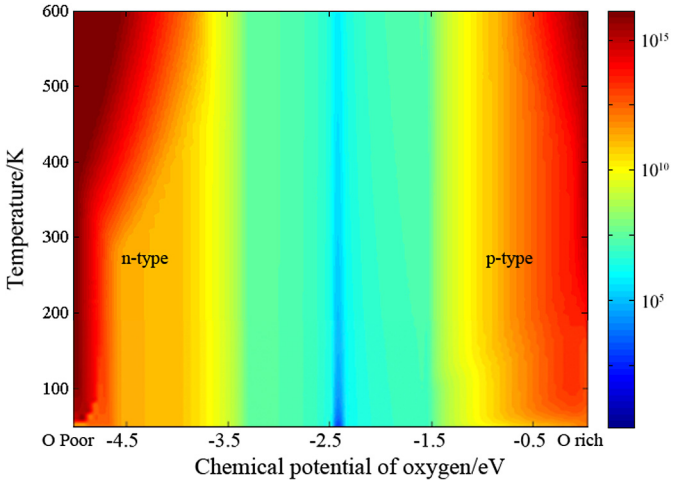

Fig. 5. (Color online.) The calculated net carrier concentrations in intrinsic MnO with respect to the chemical potential of oxygen and temperature.

3.3. Electronic properties of MnO

Based on earlier discussion, we find that V_O and the O_i are easily formed in MnO with low formation energies, and act as the dominate defects, respectively. To understand the conductive properties of MnO, we further investigate the electronic and structural properties of those two defects.

The band structures of V_O and O_i with zero and monovalence are calculated, as shown in Fig. 6. The solid and dashed lines represent the band levels with spin up and down, respectively. A well-defined direct band gap exists at the gamma point. In V_O^0, defect levels are found to be well-localized near the VBM, indicating large effective masses of the unpaired electrons contributing by the dangling bonds. Four defect levels, which are two spin up and two spin down, are well degenerated. In the case of V_O^+, as one electron is removed, the unoccupied level experiences an energy increasing and rises above the Fermi level, moving into the deep region of the band gap. For the case of O_i^0, two unoccupied defect levels derived from the interstitial O are created, locating deep into the band gap. Both the occupied and unoccupied defect levels are shown spin polarized. As the interstitial O is ionized to be O_i^-, one unoccupied defect level has captured an electron, falling down below the Fermi level. In addition, the well-localized defect levels imply a large effective mass for the electrons, and thus corresponding for a weak conductive ability.

The spin charge densities of MnO with V_O and O_i in neutral and monovalent charged states are shown in Figs. 7(a) to 7(d). The solid and dashed lines stand for the charge density contours with spin polarized up and down, respectively. Ionic bonding was usually expected to prevail in strong interaction of TM monoxides, so as in the MnO system. Comparing to that in V_O^0, more density contours are found to distribute near the oxygen vacancy in V_O^+, explaining the corresponding local magnetic moment of 1 μ_B. Local magnetic moments of ~0.46 and ~0.13 μ_B are found to distribute around the O sites for O_i^- and O_i^0, respectively. For O_i^-, a total magnetic moment of 1 μ_B per supercell is left and contributed by the defect induced magnetic polarization of O sites and the cation Mn sites. However, the collective magnetism may not exists due to the possible AFM coupling of different defects. No collective magnetic moment is found in the case of O_i^0 since the defect induced magnetic moment around the O sites and the interstitial sites is canceled out by that in Mn sites.

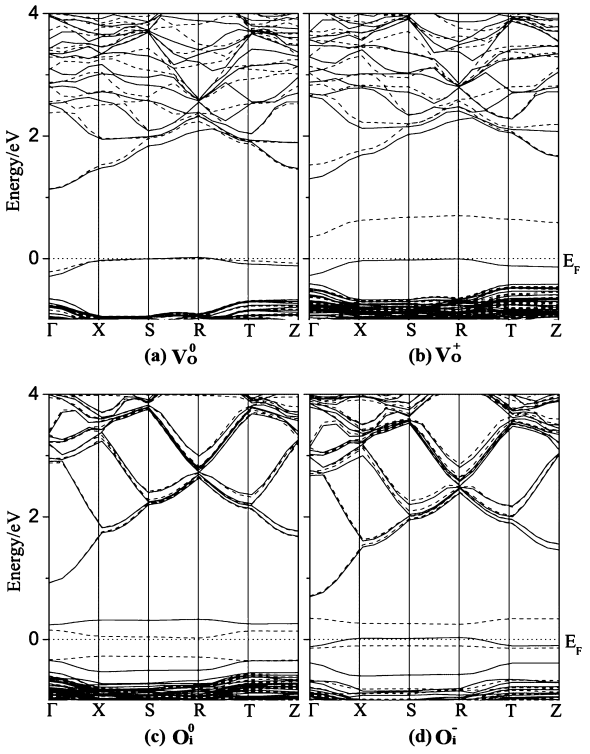

Fig. 6. The spin polarized band structures of MnO with defect of V_O^0 (a), V_O^+ (b), O_i^0 (c), or O_i^- (d). The solid and dashed lines represent the band states of the majority and minority channels, respectively.

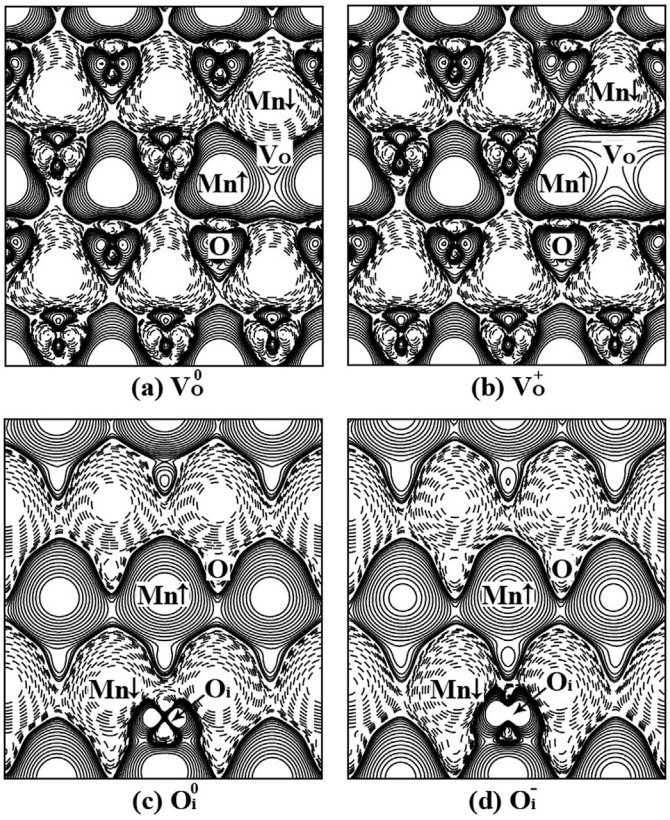

Fig. 7. The spin charge density of MnO on (001) with V_O^0 (a), V_O^+ (b), O_i^0 (c), and O_i^- (d). The solid and dashed lines represent the charge densities of the spin up and down densities, respectively, with the contours start from $0.001e$ Å^{-3} and increase successively by a factor of $\sqrt{2}$.

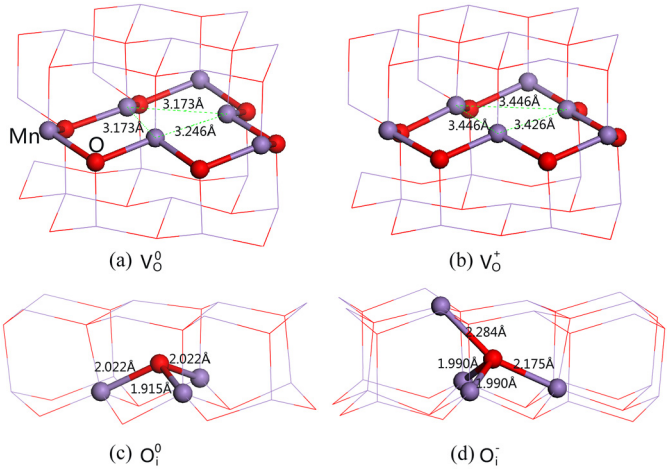

Fig. 8. (Color online.) The relaxed local structures of V_O^0 (a), V_O^+ (b), O_i^0 (c), and O_i^- (d) in WZ MnO.

3.4. Structural properties of MnO

Figs. 8(a) to 8(d) illustrate the structural properties of those two defects. As the oxygen vacancy formed, dangling bonds appear at the four surrounding Mn ions. For V_O^0 (Fig. 8(a)), the nearest-neighbor Mn ions are relaxed inward by about 0.208 to 0.233 Å. For V_O^+ (Fig. 8(b)), it undergoes a more complicated situation with two nearest-neighbor Mn ions relaxed outward by about 0.02 Å, while another one moving inward by about 0.01 Å. For O_i^0, as shown in Fig. 8(c), the interstitial oxygen is departed from the oxygen octahedral center and interacting with three surrounded Mn ions with the bond lengths be 1.195, 2.022 and 2.022 Å, respectively. In the case of O_i^- (Fig. 8(d)), comparing to O_i^0, the interstitial oxygen continues to move away from the symmetric center and forming four Mn–O bonding with their lengths be 1.190 to 2.284 Å, respectively.

4. Conclusions

We have considered the formations of both point defect and defect complexes in wurtzite CoO and MnO under O rich and O poor conditions. The Fermi levels determined by the self-consistent calculations show that MnO could easily realized *p*-type and *n*-type conductivity under O rich and O poor condition, respectively, while CoO could easily be *p*-type conductivity under O rich condition, but hard to be *n*-type. The calculated carrier concentrations of MnO are as high as 10^{17} cm^{-3} under O-rich or poor condition at room temperature. The good controllable p/n conductivity of MnO implies a new promising wurtzite semiconductor materials.

Acknowledgement

This work is supported by NSFC (Grant No. 11174082), and the Fundamental Research Funds for the Central Universities (Grant Nos. 2013ZZ0082 and 2013ZM108). The computer times at National Supercomputing Center in Shenzhen (NSCCSZ) and ScGrid of the Supercomputing Center, Computer Network Information Center of CAS are gratefully acknowledged.

References

[1] W.L. Roth, Phys. Rev. 110 (1958) 1333.
[2] W.S. Seo, J.H. Shim, S.J. Oh, E.K. Lee, N.H. Hur, J.T. Park, J. Am. Chem. Soc. 127 (2005) 6188.
[3] M.J. Redman, E.G. Steward, Nature 193 (1962) 867.
[4] K.M. Nam, Y.I. Kim, Y. Jo, S.M. Lee, B.G. Kim, R. Choi, S.I. Choi, H. Song, J.T. Park, J. Am. Chem. Soc. 134 (2012) 8392.
[5] D.C. Look, Mater. Sci. Eng. B 80 (2001) 383.
[6] D.C. Look, J. Electron. Mater. 35 (2006) 1299.
[7] Ü. Özgür, Y.I. Alivov, C. Liu, A. Teke, M.A. Reshchikov, S. Doğan, V. Avrutin, S.J. Cho, H. Morkoç, J. Appl. Phys. 98 (2005) 041301.
[8] J. Isberg, J. Hammersberg, E. Johansson, T. Wikstrom, D.J. Twitchen, A.J. Whitehead, S.E. Coe, G.A. Scarsbrook, Science 297 (2002) 1670.
[9] S. Koizumi, K. Watanabe, M. Hasegawa, H. Kanda, Science 292 (2001) 1899.
[10] D.C. Look, G.M. Renlund, R.H. Burgener, J.R. Sizelove, Appl. Phys. Lett. 85 (2004) 5269.
[11] D.C. Look, B. Claflin, Phys. Status Solidi (b) 241 (2004) 624.
[12] S.B. Zhang, S.-H. Wei, A. Zunger, Physica B 273–274 (1999) 976.
[13] S.B. Zhang, S.-H. Wei, A. Zunger, J. Appl. Phys. 83 (1998) 3192.
[14] Y. Yan, S.-H. Wei, Phys. Status Solidi (b) 245 (2008) 641.
[15] F. Oba, A. Togo, I. Tanaka, Phys. Rev. B 77 (2008) 245202.
[16] A. Janotti, C.G. Van de Walle, Phys. Rev. B 76 (2007) 165202.
[17] R. Vidya, P. Ravindran, H. Fjellvåg, B.G. Svensson, E. Monakhov, M. Ganchenkova, R.M. Nieminen, Phys. Rev. B 83 (2011) 045206.
[18] Y. Yan, J. Li, S.-H. Wei, M.M. Al-Jassim, Phys. Rev. Lett. 98 (2007) 135506.
[19] A.S. Risbud, L.P. Snedeker, M.M. Elcombe, A.K. Cheetham, R. Seshadri, Chem. Mater. 17 (2005) 834.
[20] J. Li, S.-H. Wei, S.-S. Li, J.-B. Xia, Phys. Rev. B 74 (2006) 081201.
[21] F. Oba, M. Choi, A. Togo, A. Seko, I. Tanaka, J. Phys. Condens. Matter 22 (2010) 384211.
[22] P.E. Blöchl, Phys. Rev. B 50 (1994) 17953.
[23] G. Kresse, J. Hafner, Phys. Rev. B 47 (1993) 558.
[24] G. Kresse, J. Furthmüller, Phys. Rev. B 54 (1996) 11169.
[25] G. Kresse, D. Joubert, Phys. Rev. B 59 (1999) 1758.
[26] J.P. Perdew, K. Burke, M. Ernzerhof, Phys. Rev. Lett. 77 (1996) 3865.
[27] R. Hanafin, T. Archer, S. Sanvito, Phys. Rev. B 81 (2010) 054441.
[28] S.B. Zhang, S.-H. Wei, A. Zunger, Phys. Rev. Lett. 78 (1997) 4059.
[29] S.B. Zhang, S.-H. Wei, A. Zunger, H. Katayama-Yoshida, Phys. Rev. B 57 (1998) 9642.
[30] C. Persson, Y.-J. Zhao, S. Lany, A. Zunger, Phys. Rev. B 72 (2005) 035211.
[31] Y.-J. Zhao, C. Persson, S. Lany, A. Zunger, Appl. Phys. Lett. 85 (2004) 5860.
[32] R. Sakuma, F. Aryasetiawan, Phys. Rev. B 87 (2013).
[33] Z. Szotek, W. Temmerman, H. Winter, Phys. Rev. B 47 (1993) 4029.
[34] A. Schrön, C. Rödl, F. Bechstedt, Phys. Rev. B 82 (2010) 165109.
[35] J.-M. Wu, X.-Y. Chen, S.-Y. Lin, Y.-J. Zhao, J. Appl. Phys. 114 (2013) 083905.